

₁ Study of neutrino-nucleus interaction at around 1 GeV using
₂ a 3D grid-structure neutrino detector, WAGASCI, muon
₃ range detectors and magnetized spectrometer, Baby MIND,
₄ at J-PARC neutrino monitor hall

₅ A. Bonnemaison, R. Cornat, L. Domine, O. Drapier, O. Ferreira, F. Gastaldi,
₆ M. Gonin, J. Imber, M. Licciardi, F. Magniette, T. Mueller, L. Vignoli, and O. Volcy
₇ *Ecole Polytechnique, IN2P3-CNRS, Laboratoire Leprince-Ringuet, Palaiseau,*
₈ *France*

₉ S. Cao and T. Kobayashi

₁₀ *High Energy Accelerator Research Organization (KEK), Tsukuba, Ibaraki, Japan*

₁₁ M. Khabibullin, A. Khotjantsev, A. Kostin, Y. Kudenko, A. Mefodiev, O. Mineev,
₁₂ S. Suvorov, and N. Yershov

₁₃ *Institute for Nuclear Research of the Russian Academy of Sciences, Moscow, Russia*

₁₄ B. Quilain

₁₅ *Kavli Institute for the Physics and Mathematics of the Universe (WPI), The*
₁₆ *University of Tokyo Institutes for Advanced Study, University of Tokyo, Kashiwa,*
₁₇ *Chiba, Japan*

₁₈ T. Hayashino, A. Hiramoto, A.K. Ichikawa, K. Nakamura, T. Nakaya, K Yasutome,
₁₉ and K. Yoshida

₂₀ *Kyoto University, Department of Physics, Kyoto, Japan*

₂₁ Y. Azuma, J. Harada, T. Inoue, K. Kin, N. Kukita, S. Tanaka, Y. Seiya,
₂₂ K. Wakamatsu, and K. Yamamoto

₂₃ *Osaka City University, Department of Physics, Osaka, Japan*

²⁴ A. Blondel, F. Cadoux, Y. Favere, E. Noah, L. Nicola, and S. Parsa

²⁵ *University of Geneva, Section de Physique, DPNC, Geneva, Switzerland*

²⁶ N. Chikuma, F. Hosomi, T. Koga, R. Tamura, and M. Yokoyama

²⁷ *University of Tokyo, Department of Physics, Tokyo, Japan*

²⁸ Y. Hayato

²⁹ *University of Tokyo, Institute for Cosmic Ray Research, Kamioka Observatory,
30 Kamioka, Japan*

³¹ Y. Asada, K. Matsushita, A. Minamino, K. Okamoto, and D. Yamaguchi

³² *Yokoyama National University, Faculty of Engineering, Yokoyama, Japan*

³³ December 10, 2017

³⁴ 1 Introduction

³⁵ The understanding of neutrino-nucleus interactions in the 1 GeV energy region is critical
³⁶ for the success of accelerator-based neutrino oscillation experiments such as the T2K exper-
³⁷ iment. Complicated multi-body effects of nuclei render this understanding difficult. The
³⁸ T2K near detectors have been measuring these and significant progress has been achieved.
³⁹ However, the understanding is still limited. One of the big factors preventing from full
⁴⁰ understanding is the non-monochromatic neutrino beam spectrum. Measurements with
⁴¹ different but some overlapping beam spectra would greatly benefit to resolve the contri-
⁴² bution from different neutrino energies. We, the Wagasci collaboration, proposes to study
⁴³ the neutrino-nucleus interaction at the B2 floor of the neutrino monitor building, where
⁴⁴ different neutrino spectra can be obtained due to the different off-axis position. Our exper-
⁴⁵ imental setup contains 3D grid-structure plastic-scintillator detectors filled with water as
⁴⁶ the neutrino interaction target (Wagasci modules), two side- and one downstream- muon
⁴⁷ range detectors(MRD's). The 3D grid-structure and side-MRD's allows a measurement of
⁴⁸ wider-angle scattering than the T2K off-axis near detector (ND280). High water to scintil-
⁴⁹ lator material ratio enables the measurement of the neutrino interaction on water, which
⁵⁰ is highly desired for the T2K experiment because it's far detector, Super-Kamiokande,

51 is composed of water. The MRD's consist of plastic scintillators and iron plates. The
52 downstream-MRD, so called the Baby MIND detector, also works as a magnet and pro-
53 vides the charge identification capability as well as magnetic momentum measurement for
54 high energy muons. The charge identification is essentially important to select antineu-
55 trino events in the antineutrino beam because contamination of the neutrino events is as
56 high as 30%. Most of the detectors has been already constructed. The Wagasci modules
57 have been commissioned as the J-PARC T59 experiment and the Baby MIND detector was
58 commissioned at the CERN neutrino platform. Therefore, the collaboration will be ready
59 to proceed to the physics data taking for the T2K beam time in January 2019. We will
60 provide the cross sections of the charged current neutrino and antineutrino interactions on
61 water with slightly higher neutrino energy than T2K ND280 with wide angler acceptance.
62 When combined with ND280 measurements, our measurement would greatly improve the
63 understanding of the neutrino interaction at around 1 GeV and contribute to reduce one
64 of the most significant uncertainty of the T2K experiment.

65 **2 Experimental Setup**

66 Figure. 1 shows a schematic view of the entire set of detectors. A central detector, Wagasci
67 modules, consists of 3D grid-structure plastic-scintillator detectors filled with water as the
68 neutrino interaction target. They are surrounded by two side- and one downstream- muon
69 range detectors(MRD's) The MRD's are used to select muon tracks from the charged-
70 current (CC) interactions and to reject short tracks caused by neutral particles that orig-
71 inate mainly from neutrino interactions in material surrounding the central detector, like
72 the walls of the detector hall, neutrons and gammas, or neutral-current (NC) interactions.
73 The muon momentum can be reconstructed from its range inside the detector. The MRD's
74 consist of plastic scintillators and iron plates. In addition, each of the iron plates of the
75 downstream-MRD, so called the Baby MIND detector, is wound by a coil and can be
76 magnetized. It provide the charge selection capability.

77 For all detectors, scintillation light in the scintillator bar is collected and transported
78 to a photodetector with a wavelength shifting fiber (WLS fiber). The light is read out by
79 a photodetector, Multi-Pixel Photon Counter (MPPC), attached to one end of the WLS
80 fiber. The signal from the MPPC is read out by the dedicated electronics developed for the
81 test experiment to enable bunch separation in the beam spill. The readout electronics is
82 triggered using the beam-timing signal from MR to synchronize to the beam. The beam-
83 timing signal is branched from those for T2K, and will not cause any effect on the T2K
84 data taking.

85 T2K adopted the off-axis beam method, in which the neutrino beam is intentionally
86 directed 2.5 degrees away from SK producing a narrow band ν_μ beam. The off-axis near
87 detector, ND280, is installed towards the SK direction in the B1 floor of the near detector
88 hall of the J-PARC neutrino beam-line. We propose to install our detector in the B2 floor

tmp.pdf

Figure 1: Schematic view of entire sets of detectors.

89 of the near detector hall, where the off-axis angle is similar but slightly different: 1.5 degree.
90 The candidate detector position in the B2 floor is shown in Fig. 2. The expected neutrino
91 energy spectrum at the candidate position is shown in Fig. 3.

92 **2.1 Wagasci module**

93 The dimension of the central detector is 100cm \times 100cm in the x and y directions and
94 200cm along the beam direction. The total water and hydrocarbon masses serving as
95 neutrino targets are \sim 1 ton each. Inside the central detector, plastic scintillator bars are
96 aligned as a 3D grid-like structure, shown in Fig. 4, and spaces in the structure are filled
97 with the neutrino target materials, water and hydrocarbon. When neutrinos interact with
98 hydrogen, oxygen or carbon, in water and hydrocarbon, charged particles are generated.
99 Neutrino interactions are identified by detecting tracks of charged particles through plastic
100 scintillation bars. Thanks to the 3 D grid-like structure of the scintillator bars, the central
101 detector has 4π angular acceptance for charged particles. Furthermore, adopting a 2.5cm
102 grid spacing, short tracks originated from protons and charged pions can be reconstructed
103 with high efficiency. Thin plastic scintillator bars (thickness \sim 0.3cm) will be used for the
104 central detector to reduce the mass ratio of scintillator bars to neutrino target materials,
105 because neutrino interactions in the scintillator bars are a background for the cross section
106 measurements. Scintillator bars whose dimensions are 2.5cm \times 0.3cm \times 100cm will be used
107 for the central detector. The total number of channels in the central detector is 12880.

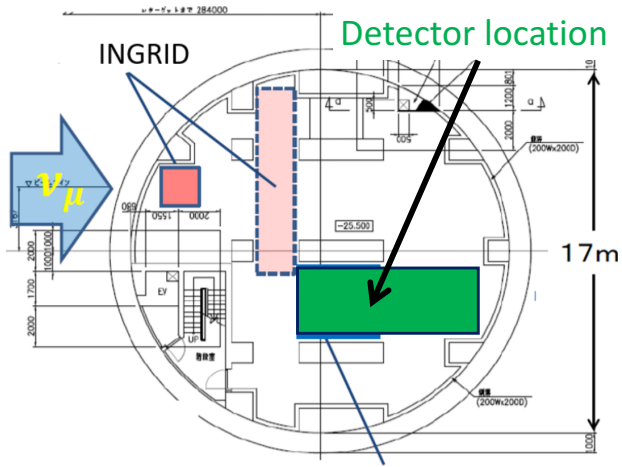


Figure 2: Candidate detector position in the B2 floor of the near detector hall.

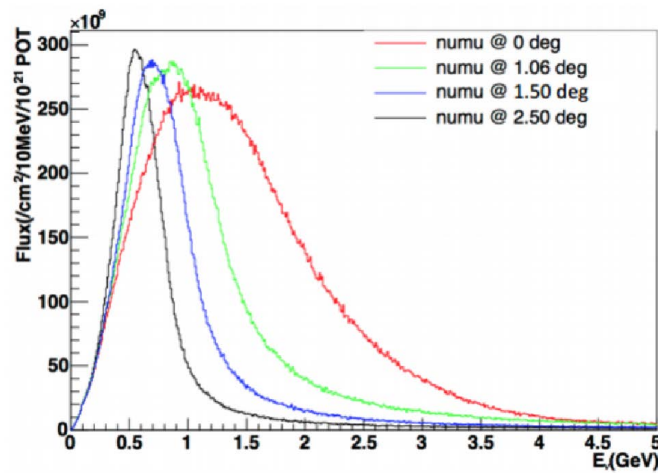


Figure 3: Neutrino energy spectrum at the candidate detector position(red, off-axis 1.5 degree). The spectrum at the ND280 site (black, off-axis 2.5 degree) is also shown.

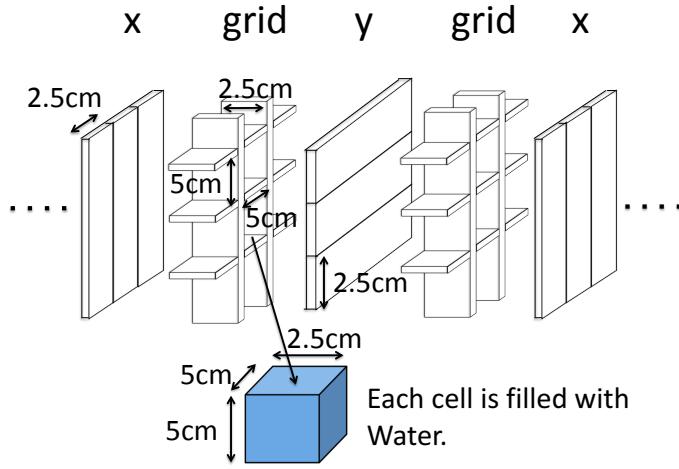


Figure 4: Schematic view of 3D grid-like structure of plastic scintillator bars inside the central detector.

108 2.2 Baby MIND

109 The Baby MIND is the downstream Muon Range Detector. It also works as a magnet and
110 provides the charge identification capability as well as magnetic momentum measurement
111 for high energy muons.

112 The Baby MIND collaboration ¹ submitted a proposal to the SPSC at CERN, SPSC-P-
113 353 [1], written to outline project plans with a focus on construction and testing activities
114 at CERN. The project was approved by the CERN research board as Neutrino Platform
115 project NP05. The detector consists of 33 magnet modules, each 3500 mm × 2000 mm ×
116 50 mm (30 mm steel) with a mass of approximately 2 tonnes. Of these magnet modules,
117 18 are instrumented with plastic scintillator modules.

118 2.2.1 Magnet modules

119 The Baby MIND is built from sheets of iron interleaved with scintillator detector modules
120 but unlike traditional layouts for magnetized iron neutrino detectors (e.g. MINOS) which
121 tend to be monolithic blocks with a unique pitch between consecutive steel segments and
122 large conductor coils threaded around the whole magnet volume, the Baby MIND iron
123 segments are all individually magnetized, allowing for far greater flexibility in the setting
124 of the pitch between segments, and in the allowable geometries that these detectors can
125 take.

¹Contact person: E. Noah, Spokesperson: A. Blondel, Deputy spokesperson: Y. Kudenko

126 The key design outcome is a highly optimized magnetic field map. A double-slit con-
 127 figuration for coil winding was adopted to increase the area over which the magnetic flux
 128 lines are homogeneous in B_x across the central tracking region. Simulations show the
 129 magnet field map to be very uniform over this central tracking region covering an area of
 130 $2800 \times 2000 \text{ mm}^2$, Figure 5. The B_x component dominates in this region, with negligible
 131 B_y and B_z . This was confirmed by measuring the field with 9 pick-up coils wound around
 132 the first ARMCO module. Subsequent modules were equipped with one pick-up coil. Test
 133 results on the 33 modules show all to achieve the required field of 1.5 T for a current of
 134 140 A, with a total power consumption of 11.5 kW. The polarity of the field map shown
 135 in Figure 5 (middle) can be reversed by changing the power supply configuration.

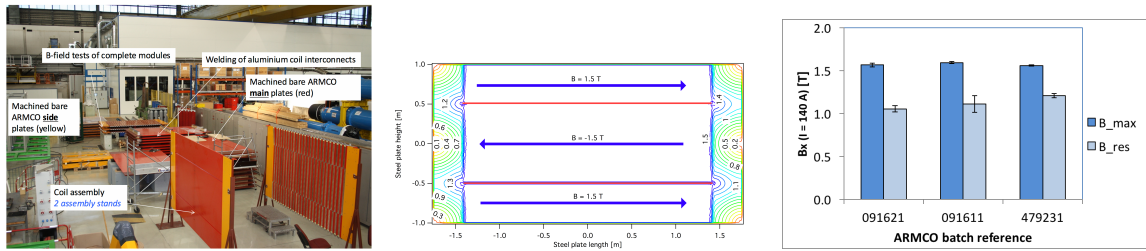


Figure 5: Left) Magnet assembly zone at CERN. Middle) Magnetic field map with a coil along 280 cm of the length of the plate. Right) Measured B field for 33 modules.

135

136 2.2.2 Scintillator modules

137 Each of the 18 scintillator modules is constructed from 2 planes of horizontal counters (95
 138 counters in total) and 2 planes of vertical counters (16 counters in total) [2], arranged
 139 with an overlap between planes to achieve close to 100% hit efficiency for minimum ionizing
 140 muons. The arrangement of planes within a module is vertical-horizontal-horizontal-
 141 vertical, with construction of each module carried out in two separate phases, one front
 142 half-module constructed with two planes vertical/horizontal, and one back half-module
 143 constructed with two further planes horizontal/vertical. The scintillator bars are held in
 144 place using structural ladders that align and maintain the counters, Figure 6. No glue is
 145 used in the process, so counters can be replaced. Aluminum sheets front and back provide
 146 light tightness.

147 The plastic scintillator counters were made from 220 mm-wide slabs, consisting of
 148 extruded polystyrene doped with 1.5% paraterphenyl (PTP) and 0.01% POPOP. They were
 149 cut to size then covered with a 30-100 μm thick diffuse reflector resulting from etching of
 150 the surface with a chemical agent [3, ?]. The horizontal counter size is $2880 \times 31 \times 7.5 \text{ mm}^3$,
 151 with one groove along the length of the bar in which sits a wavelength shifting fiber from
 152 Kuraray. The vertical counter size is $1950 \times 210 \times 7.5 \text{ mm}^3$, with one U-shaped groove
 153 along the bar. On each counter, two custom connectors house silicon photomultipliers,



Figure 6: Scintillator modules assembly. Left) top of front half-module showing vertical counters, and the spacers-ladders that set the pitch between horizontal counters and hold them in place. Middle) rear half-module showing horizontal counters on their ladders. Right) Assembled rear half-module, the front half-module can be seen in the background.

154 MPPC type S12571-025C from Hamamatsu, either side of the horizontal counter, and
 155 both connectors at the top for the vertical counter. This geometrical configuration for
 156 vertical counters was chosen for ease of connectivity to the electronics, and maintenance
 157 operations.

158 A total of 1744 horizontal counters and 315 vertical counters (including spares) were
 159 produced at the Uniplast company (Vladimir, Russia).

160 2.2.3 Electronics

161 The Baby MIND electronic readout scheme includes several custom-designed boards [4].
 162 The revised version is shown in Figure 7. At the heart of the system is the electronics
 163 Front End Board (FEB), developed by the University of Geneva. The readout system
 164 includes two ancillary boards, the Backplane, and the Master Clock Board (MCB) whose
 165 development has been managed by INRNE (Bulgarian Academy of Sciences) collaborators.

166 The FEBv2 hosts 3 CITIROC chips that can each read in signals from 32 SiPMs
 167 [5]. Each signal input is processed by a high gain, and a separate low gain, signal path.
 168 Both paths comprise independent pre-amplification and "slow" shaping stages with tunable
 169 gain and shaping time constant, respectively. The outputs from the slow shapers can be
 170 sampled using one of two modes: a mode with an externally applied delay, and a peak
 171 detector mode. A faster shaper can be switched to either HG or LG paths, followed by
 172 discriminators with adjustable thresholds providing 32 individual trigger outputs and one
 173 OR32 trigger output. An Altera ARIA5 FPGA on the FEBv2 samples these trigger outputs
 174 at 400 MHz, recording rising and falling times for the individual triggers and assigning
 175 time stamps to these. Time-over-threshold from the difference between falling and rising
 176 times gives some measure of signal amplitude, used in addition to charge information and
 177 useful if there is more than one hit per bar within the deadtime due to the readout of the
 178 multiplexed charge output of $\sim 9 \mu\text{s}$. The ARIA5 also manages the digitization of the
 179 sampled CITIROC multiplexed HG and LG outputs via a 12-bit 8-ch ADC.

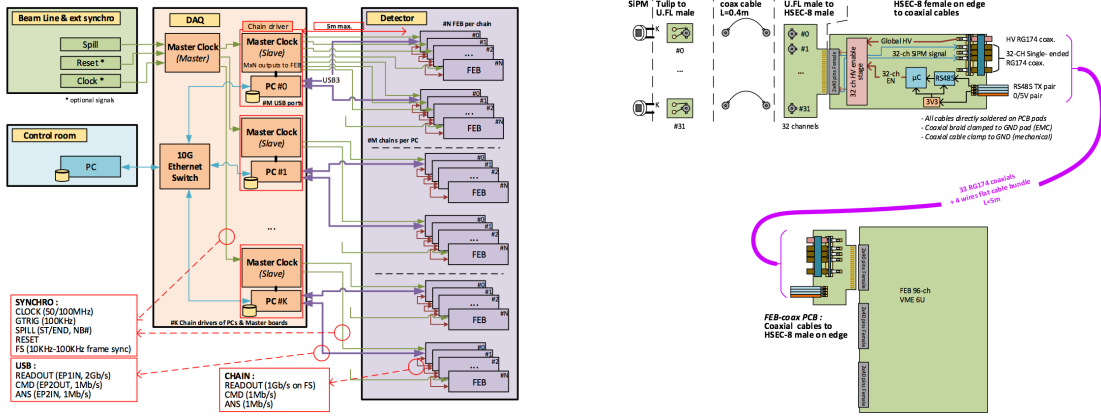


Figure 7: Left) Baby MIND electronics readout scheme. Right) SiPM-to-FEB connectivity.

180 The internal 400 MHz clock on the FEBv2 can be synchronized to a common 100 MHz
 181 clock. The synchronization subsystem combines input signals from the beam line into
 182 a digital synchronization signal (SYNC) and produces a common detector clock (CLK)
 183 which can eventually be synchronised to an external experiment clock [6]. Both SYNC
 184 and CLK signals are distributed to the FEBs. Tests show the FEB-to-FEB CLK(SYNC)
 185 delay difference to be 50 ps (70 ps). Signals from the beam line at WAGASCI include two
 186 separate timing signals, arriving 100 ms and 30 μ s before the neutrino beam at the near
 187 detectors [7]. The spill number is available as a 16-bit signal.

188 References

- 189 [1] M. Antonova *et al.* CERN-SPSC-2015-031, SPSC-P-353.
- 190 [2] M. Antonova *et al.* [Baby MIND Collaboration], arXiv:1704.08917 [physics.ins-det].
- 191 [3] Y. G. Kudenko, L. S. Littenberg, V. A. Mayatsky, O. V. Mineev and N. V. Ershov,
 192 Nucl. Instrum. Meth. A **469** (2001) 340. doi:10.1016/S0168-9002(01)00780-X
- 193 [4] E. Noah *et al.*, PoS PhotoDet **2015** (2016) 031.
- 194 [5] J. Fleury, S. Callier, C. de La Taille, N. Seguin, D. Thienpont, F. Dulucq, S. Ahmad
 195 and G. Martin, JINST **9** (2014) C01049. doi:10.1088/1748-0221/9/01/C01049
- 196 [6] G. Mitev, Y. Favre *et al.*, "Synchronization of the distributed readout frontend elec-
 197 tronics of the Baby MIND detector", Proc. XXVI International Scientific Conference
 198 Electronics - ET2017, Sozopol, Bulgaria, 2017.

199 [7] N. Chikuma *et al.*, "Development of electronics and data acquisition system for the
200 J-PARC T59 (WAGASCI) experiment", PoS EPS-HEP2017 (2017).

201 **2.3 Side muon range detector**

202 Four Side-MRD modules for tracking secondary particles from neutrino interactions will
203 be constructed by the end of January 2018. Each Side-MRD module is composed of 11
204 steel plates and 10 layers of total 80 scintillator slabs installed in 13 mm gaps between the
205 30 mm thick plates. Each steel plate size is $30 \times 1610 \times 1800$ mm 3 . Total module size is
206 $2236 \times 1630 \times 975$ mm 3 as shown in Fig. 8, weight is ~ 8.5 ton.

207 Scintillator bars were manufactured by Uniplast company in Vladimir, Russia. Polystyrene
208 based scintillators were extruded with thickness of 7 mm, then cut to the size of $7 \times 200 \times$
209 1800 mm 3 . Dopant composition is 1.5% PTP and 0.01% POPOP. Scintillator surface was
210 etched by a chemical agent to form a white diffuse layer with excellent reflective perfor-
211 mance. Ideal contact between the scintillator and the reflector raises the light yield up to
212 50% comparing to an uncovered scintillator. Sine like groove was milled along the scin-
213 tillator to provide uniform light collection over the whole scintillator surface. WLS Y11
214 Kuraray fiber of 1 mm diameter is glued with an optical cement EJ-500 in the S-shape
215 groove as shown in Fig. 9. Bending radius is fixed to 30 mm that was specified to be safe
216 for Kuraray S-type fibers. Both ends of the fiber are glued into optical connectors (Fig.
217 10) which mounted within a scintillator body.

218 The plastic molded connectors provide an interface to SiPMs, Hamamatsu MPPC
219 S13081-050CS(X1) used for the WAGASCI detector. Optical coupler of this type (so-called
220 Baby-mind type of optical connector) consists of two parts (see Fig. 10): an container for
221 the MPPC and a ferrule with the fiber. The ferrule is glued in the scintillator, and its end
222 with glued in WLS fiber was polished. Both parts of the optical coupler are latched by a
223 snap-like mechanism: a locking groove inside the container and matching ring protuber-
224 ance on the ferrule. To ensure the optical contact a foam spring made of sponge rubber
225 presses the MPPC to the fiber end (Fig. 11).

226 Scintillators for the Side-MRD modules had been assembled at INR in Russia, and
227 shipped to Japan in July 2017. The light yield for each scintillator was measured with
228 cosmic rays at INR and at YNU in Japan after delivery. Parameters measured at the
229 center of the counter were : the light yields LY_1 and LY_2 at both ends, the light yield
230 asymmetry between the ends calculated as $100\% \times \frac{LY_1 - LY_2}{LY_1 + LY_2}$. After tests at INR we selected
231 324 counters from measured 332 ones with the mean light yield of 45 p.e./MIP ($LY_1 + LY_2$)
232) and the asymmetry value less than 10 %. The measuremens at YNU yielded the average
233 total light yield of about 40 p.e./MIP which varies in range from 32 to 50 p.e./MIP (Fig.
234 12 (left)). Only two counters showed relatively high asymmetry close to 25 % as shown in
235 Fig. 12 (right). Using the results of the quality assurance test we selected 320 scintillator
236 counters for the Side-MRD modules.

237 We also measured the time resolution for a combination of four counters piled each on

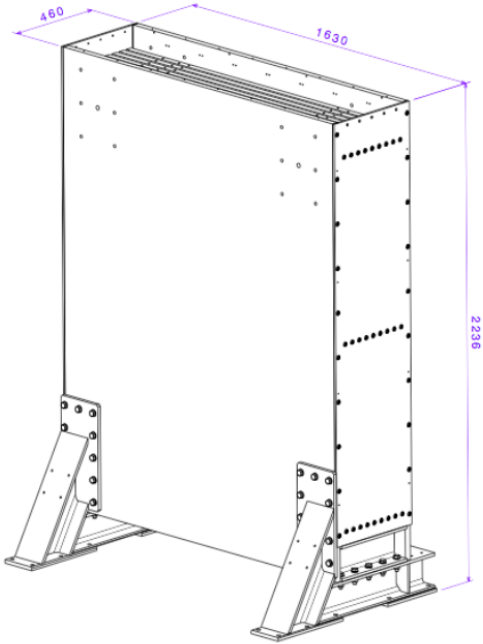


Figure 8: Support structure of the Side-MRD module.

another one. Time resolution for a single counter is determined as rms of $(T_{left} - T_{right})/2$ distribution. The difference of times was chosen to remove the correlated time fluctuation caused by a start trigger signal. The average result for four counters is $\sigma_T = 1.04$ ns (Upper left plot in Fig. 13). For a set of n counters the time resolution is calculated as $\frac{(T_L - T_R)_1 + (T_L - T_R)_2 + \dots + (T_L - T_R)_n}{2 \times n}$. The result of combination of 2, 3, 4 counters is 0.79 ns, 0.66 ns and 0.58 ns, correspondently (Fig. 13).

Construction of Side-MRD modules will be done from November 2017 to January 2018 at Yokohama National University, then they will be transported to J-PARC and will be installed at B2 floor of the T2K near detector hall before T2K beam in March 2018.

3 Physics goals

We will measure the differential cross section for the charged current interaction on H₂O and Hydrocarbon(CH)). The water-scintillator mass ratio of the Wagasci module is as high as 5:1 and the high purity measurement of the cross section on H₂O is possible. One experimental option is to remove water from one of the two Wagasci modules. The water-out WAGASCI module will allow to measure pure-CH target interactions with very low

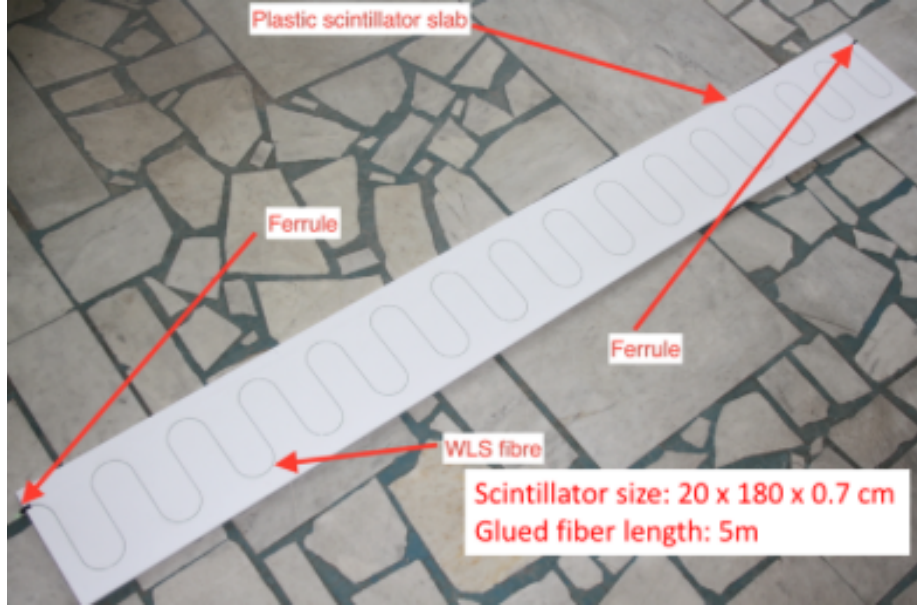


Figure 9: Scintillator bar of the Side-MRD modules.

253 momentum-threshold for protons. It will also benefit to subtract the background from
 254 interaction with scintillator in the water target measurement. Another option is to add
 255 the T2K proton module which is fully made of plastic scintillators. It will allow the high
 256 statistics comparison of cross section between H₂O and CH and also comparison with
 257 the ND280 measurement. The actual configuration will be optimized with detailed MC
 258 simulation by 2018 Summer.

259 Our setup allows the measurements of inclusive and also exclusive channels such as 1- μ ,
 260 1- μ 1p, 1- μ 1 π \pm np samples, former two of which are mainly caused by the quasi-elastic and
 261 2p2h interaction and the latter is mainly caused by resonant or coherent pion production
 262 and deep elastic scattering. In general, an accelerator produced neutrino beam spectrum
 263 is wide and the energy reconstruction somehow rely on the neutrino interaction model.
 264 Therefore, recent neutrino cross section measurement results including those from T2K
 265 are given as a flux-integrated cross section rather than cross sections as a function of
 266 the neutrino energy to avoid the model dependency. We can provide the flux-averaged
 267 cross section. In addition, by combining our measurements with those at ND280, model-
 268 independent extraction of the cross section for narrow energy region becomes possible.
 269 This method was demonstrated in [1] and also proposed by P** (NUPRISM).

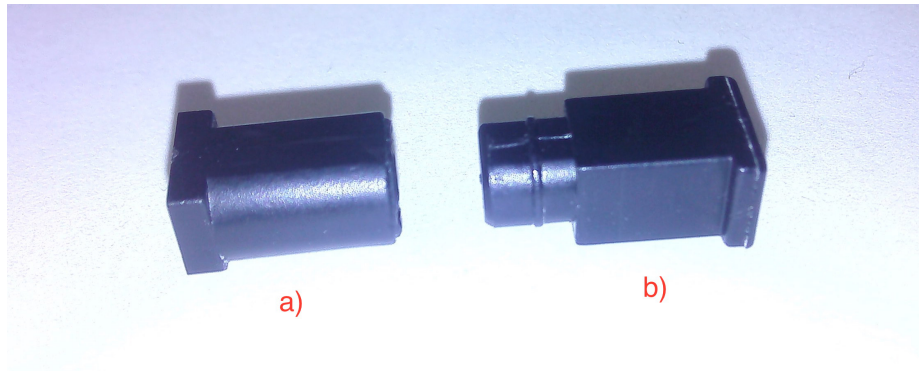


Figure 10: Optical connector for the Side-MRD scintillator. a) MPPC cover. b) Ferrule.

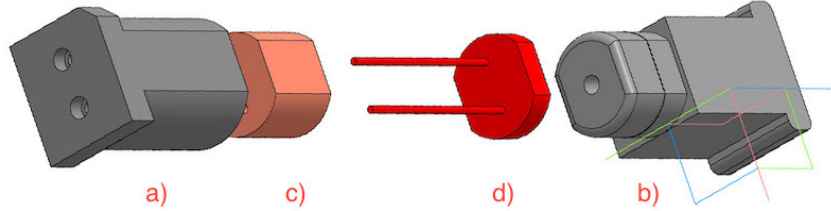


Figure 11: Scheme of the MPPC placement in optical connector. a) MPPC cover. b) Ferrule. c) Spring (sponge rubber). d) MPPC.

270 3.1 Expected number of events

271 Expected number of neutrino events after the event selections is evaluated with Monte
 272 Carlo simulations as we will discuss in Section 6. 2.41×10^4 CC events are expected in
 273 two WAGASCI modules after the selection with 1×10^{20} POT in neutrino-mode, and its
 274 purity is 75.5 %. In case we choose the option with one WAGASCI module and the T2K
 275 proton module, 1.2×10^4 CC events are expected in the WAGASCI module and $\sim 1 \times 10^4$
 276 CC events are expected in the T2K proton module. In case we choose the option with one
 277 water-in WAGASCI module and one water-out WAGASCI module, 1.2×10^4 CC events are
 278 expected in the water-in module and 0.24×10^4 CC events are expected in the water-out
 279 module.

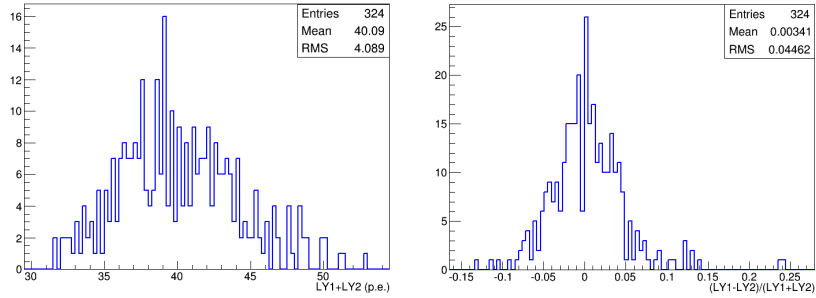


Figure 12: Total light yield distribution (left) and light yield assymetry (right) measured at YNU.

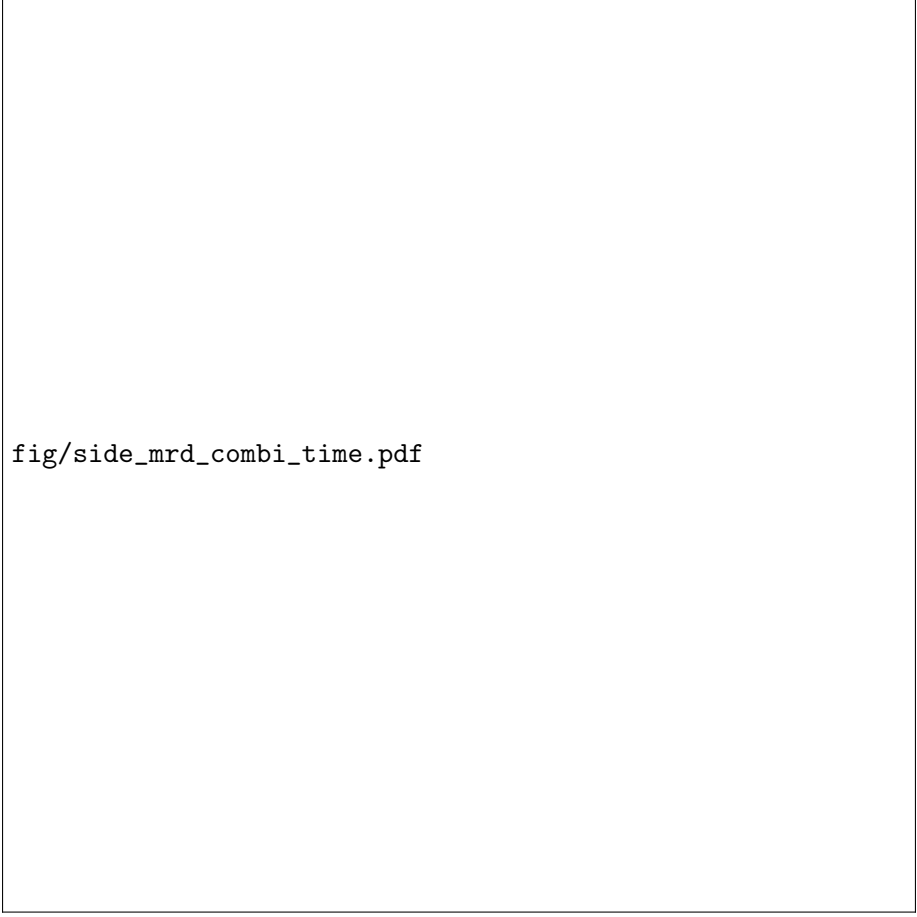
280 3.2 Pseudo-monochromatic beam by using different off-axis fluxes

281 The off-axis method gives narrower neutrino spectrum, and the peak energy is lower for
 282 larger off-axis angle. There still remains high energy tail mainly due to neutrinos from
 283 Kaon decay. The off-axis angle of the Wagasci location is 1.5 degree and different from the
 284 ND280 2.5 degree. Top two plots of Fig. 14 show the energy spectra of fluxes and neutrino
 285 interaction events at these two different location. The high energy tail of ND280 flux can
 286 be somehow subtraction by using the Wagasci measurement. The low energy part of the
 287 Wagasci flux can be also subtracted by using the ND280 measurement. Bottom two plots
 288 of Fig. 14 demonstrate this method. We can effectively get two fluxes, from 0.2 GeV to
 289 0.9 GeV and 0.6 GeV and 2 GeV and measure flux-integrated cross section for these two
 290 fluxes.

291 3.3 Subjects Wagasci can contribute

292 In T2K experiment, neutrinos interact with bound nucleons in relatively heavy nuclei
 293 (Carbon and Oxygen), so the cross-section is largely affected by nuclear effects. The nuclear
 294 effects are categorized as nucleons' momentum distribution in nucleus, interactions with
 295 correlated pairs of nucleons in nucleus (two particles-two holes, 2p2h), collective nuclear
 296 effects calculated with Random Phase Approximation (RPA) and final state interactions
 297 (FSI) of secondary particles in the nuclei after the initial neutrino interactions.

298 The 2p2h interactions mainly happen through Δ resonance interactions following a
 299 pion-less decay and interactions with a correlated nucleon pair. The 2p2h interactions are
 300 observed in electron scattering experiments (add ref. here) where the 2p2h events observed
 301 in the gap between Quasi-Elastic region and Pion-production region as shown in Fig. ???.
 302 Neutrino experiments also attempt to measure the 2p2h interactions, but separation of the
 303 QE peak and the 2p2h peak is more difficult because transferred momentum (p) and energy



```
fig/side_mrd_combi_time.pdf
```

Figure 13: Time resolution for one (upper left) and a set of 2,3,4 Side-MRD counters.

304 (w) are largely affected by neutrino energies which cannot be determined event-by-event in
305 the wide energy spectrum of the accelerator neutrino beam. Our model-independent narrow
306 neutrino spectra extracted from combined analyses of our data and ND280 data are ideal
307 for searching the 2p2h interaction because clearer separation of the QE peak and the 2p2h
308 peak is expected. Another way to observe the 2p2h interaction is direct measurement of
309 proton tracks in CC0 π sample with low detection threshold and full acceptance. Fig. ??
310 shows proton multiplicities in CCQE events and 2p2h events, and Fig. ?? shows opening
311 angles among two proton tracks in the same samples. The water-out WAGASCI can provide
312 good sample for the 2p2h interaction search because its low density medium enables the
313 detection of low momentum protons in addition to the full acceptance.

314 The corrections from collective nuclear effects calculated by RPA as a function of Q^2 are

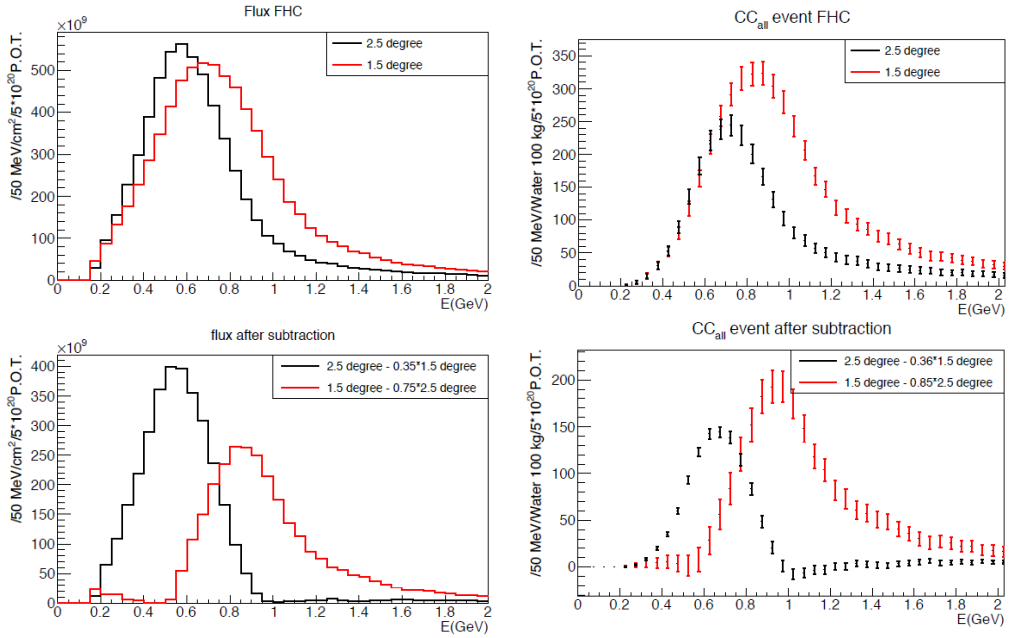


Figure 14: Energy spectra obtained by using different off-axis angle fluxes. Top two plots show the fluxes(left) and spectra of interaction events (right) for ND280 (off-axis 2.5 degree) and Wagasci (off-axis 1.5 degree). Bottom two plots show the fluxes (left) and spectra of interaction events (right) obtained by subtraction of fluxes at ND280 and Wagasci. The error bar is for the statistical error and those in the bottom right plot is obtained assuming the statistical error for ND280 measurement is much smaller than that of Wagasci experiment.

315 shown in Fig. ???. The Q^2 dependence of the correction can be tested by measuring angular
 316 distribution of muons in $\text{CC1-}\mu$ and $\text{CC1-}\mu 1p$ events. The uncertainties of the corrections
 317 in low (high) Q^2 regions can be constrained by observing the events with a forward-going
 318 (high-angle) muon, so it is essential to measure muon tracks with full acceptance.

319 T2K experiment is starting to use ν_e $\text{CC1}\pi$ events for its CP violation search to increase
 320 the statistics. One of the biggest uncertainty of the $\text{CC1}\pi$ sample comes from the final
 321 state interactions of pions in the nuclei after the initial neutrino interactions because they
 322 change the multiplicity, charge and kinematics of the pions. The multi-pion production
 323 events can be migrated into the $\text{CC1}\pi$ sample due to the FSIs, and they become important
 324 backgrounds. We can constrain the uncertainties from the pion FSIs by measuring pion
 325 rescattering in the detector and pion multiplicity in ν_μ $\text{CCn}\pi$ sample with low detection
 326 threshold and full acceptance for pion tracks. The water-out WAGASCI can provide good
 327 sample for the pion FSI studies because its low density medium enables the detection of

328 low momentum pions in addition to the full acceptance.

329 4 Status of J-PARC T59 experiment

330 We had submitted a proposal of a test experiment to test a new detector with a water
331 target, WAGASCI, at the T2K near detector hall to J-PARC PAC on April 2014, and the
332 proposal was approved as J-PARC T59. There are several updates on the project after
333 three years from then. Fist, the start time of neutrino beam measurement is changed from
334 December 2015 to October 2017, and the requested neutrino beam is changed from 1×10^{21}
335 POT of ν beam to 0.8×10^{21} POT of anti- ν beam. Second, the detector configuration is
336 changed. In the original proposal, central neutrino detector are expected to be surrounded
337 by newly developed muon-range detectors (MRDs), but we will use spare neutrino detectors
338 of the T2K experiment instead of them during neutrino beam measurement from October
339 to December 2017. Construction of the newly developed MRDs, Baby-MIND and Side-
340 MRD, is in progress, and they will be installed to the both sides and the downstream of
341 the central neutrino detector from January to March 2018. Then, we will resume neutrino
342 beam measurements from March 2018 and will take the neutrino beam data until May
343 2018.

344 4.1 On-axis beam measurement with Prototype detector

345 Add INGRID water module measurement here.

346 4.2 Plans from October 2017 to May 2018

347 J-PARC MR will extract its proton beam to T2K neutrino beam-line from October to
348 December 2017, and, from March to May 2018. T2K experiment will produce anti-neutrino
349 beam and will accumulate $\sim 8 \times 10^{20}$ POT data during the above period.

350 J-PARC T59 will perform neutrino beam measurements on the B2 floor of the T2K
351 near neutrino detector hall during the above period to test basic performances of the
352 WAGASCI detector and new electronics. During the beam measurements from October to
353 December 2017, one WAGASCI module will be placed between spare neutrino detectors of
354 the T2K experiment, INGRID Proton module and INGRID standard module. Here, the
355 INGRID Proton module is used as a charged particle VETO detector and, the INGRID
356 standard module is used as a downstream muon detector. We had submitted a proposal
357 to use these spare neutrino detectors for the T59 neutrino beam measurements to the T2K
358 collaboration, and we got an approval from T2K.

359 During the beam measurements from March to May 2018, Baby-MIND and two side
360 muon-range detector (Side-MRD) modules will be installed on the downstream and the
361 both sides of the WAGASCI detector, as shown in Fig. 15, to increase angular acceptance

362 for secondary charged particles from neutrino interactions. Add Baby-MIND commission-
363 ing items here!!!

tmp.pdf

Figure 15: J-PARC T59 detector configuration with Baby-MIND and two Side-MRD modules from Mar. to May 2018. (Need to prepare the figure.)

364 Expected number of neutrino events in the WAGASCI detector during the above beam
365 period is evaluated with Monte Carlo simulations. Neutrino beam flux at the detector
366 location is simulated by T2K neutrino flux generator, JNUBEAM, neutrino interactions
367 with target materials are simulated by a neutrino interaction simulator, NEUT, detector
368 responses are simulated using GEANT4-based simulation. The neutrino flux at the detector
369 location, 1.5 degrees away from the J-PARC neutrino beam axis, is shown in Figure 3, and
370 its mean neutrino energy is around 0.68 GeV. An event display of the GEANT4-based
371 detector simulation is shown in Figure 18.

372 To perform the detector performance test, the following event selections are applied to
373 the data. First, track reconstructions are performed in the WAGASCI detector, and the
374 reconstructed vertex is required to be inside a defined fiducial volume, $80 \times 80 \times 32 \text{ cm}^3$
375 region at the center of the detector, to reduce contamination from external backgrounds.
376 Second, at least one charged particle is required to reach to INGRID standard module
377 or Side-MRD modules, and it makes more than two hits in these sub-detectors. With the
378 event selection, expected numbers of the neutrino-candidate events during the beam period
379 are summarized in Table 1. Using the data, we will test the detector performance with
380 $\sim 3\%$ statistical uncertainties.

381 **5 Detector performance**

382 **5.1 Wagasci module**

383 To demonstrate the performance of the Wagasci module and also to study the neutrino
384 interaction, the first Wagasci module was installed at the on-axis position, in front of
385 the T2K INGRID horizontal center module in 2016. The INGRID module is made of iron
386 plates and segmented plastic scintillator bars. It's cross sectional size viewed from the beam
387 direction is $1\text{ m} \times 1\text{ m}$. The charged current interactions in the Wagasci module are selected
388 by requiring a muon track candidate in the INGRIRD modules. Here, we describe the
389 performance of the Wagasci module evaluated at this T2K on-axis measurement. Figure 16
390 shows the light yeild of channels for muons produced by the interaction of neutrinos in the
hall wall. The light yield is sufficiently hgih to get good hit efficieincy. A track search

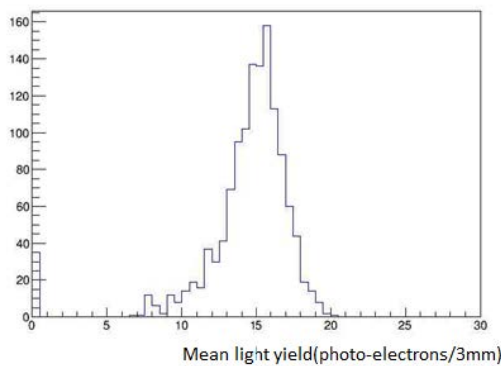


Figure 16: Light yield of channels for muons produced by the interaction of neutrinos in the hall wall.

391
392 algorithm based on the celluar automaton has been developed using the software tools by
393 the T2K INGRID. The tracking efficiency in 2-dimentional projected plane was evalualted
394 by comparing the reconstructed track in the Wagasci module and the INGRID module and
395 shown in Fig.17. Note that that the tracking efficinecy for high angle ($> 70\text{ deg}$) is not
396 evaluated because of the acceptance of the INGRID module, not because of the limitation
397 of the Wagasci module.

398 **5.2 Baby MIND**

399 The Baby MIND construction was completed in June 2017, and it was then tested in
400 June and July 2017 at the Proton Synchrotron experimental hall at CERN with a mixed

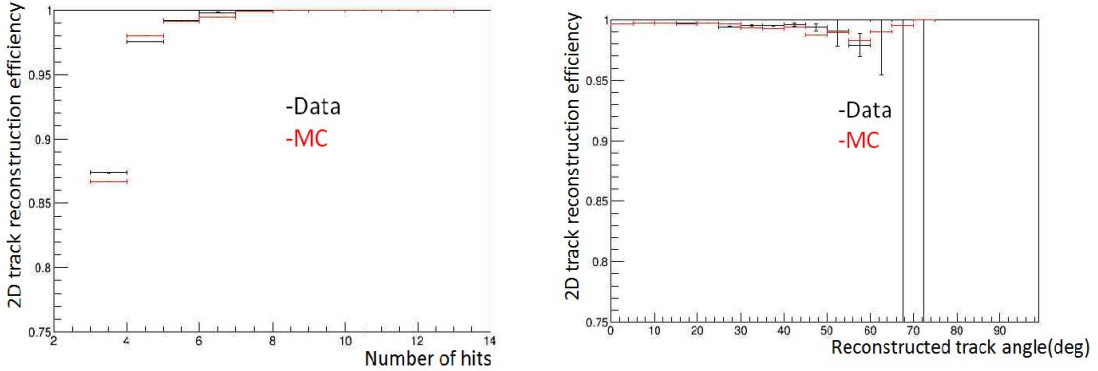


Figure 17: 2D track reconstruction efficiency as a function of number of hits (left) and track angle (right). Here the track angle is the one reconstructed by the INGRID module.

401 particle beam comprising mostly muons whose momenta could be selected between 0.5 and
 402 5 GeV/c. An event display from the summer 2017 tests is shown in Figure 20.

403 All counters were measured at INR Moscow with a cosmic ray setup using the same
 404 type S12571-025C MPPCs and CAEN DT5742 digitizer [?]. The average light yield (sum
 405 from both ends) was measured to be 37.5 photo-electrons (p.e.) per minimum ionizing
 406 particle (MIP) and 65 p.e./MIP for vertical and horizontal counters, respectively. After
 407 shipment to CERN, all counters were tested once more individually with an LED test setup
 408 [?]. 0.1% of counters failed the LED tests and were therefore not used during the assembly
 409 of modules.

410 5.3 Side muon range detector

411 6 MC studies

412 6.1 Detector simulation

413 Expected number of neutrino events in the WAGASCI detector is evaluated with Monte
 414 Carlo simulations. Neutrino beam flux at the detector location is simulated by T2K neu-
 415 trino flux generator, JNUBEAM, neutrino interactions with target materials are simu-
 416 lated by a neutrino interaction simulator, NEUT, detector responses are simulated using
 417 GEANT4-based simulation. The neutrino flux at the detector location, 1.5 degrees away
 418 from the J-PARC neutrino beam axis, is shown in Figure 3, and its mean neutrino energy
 419 is around 0.68 GeV.

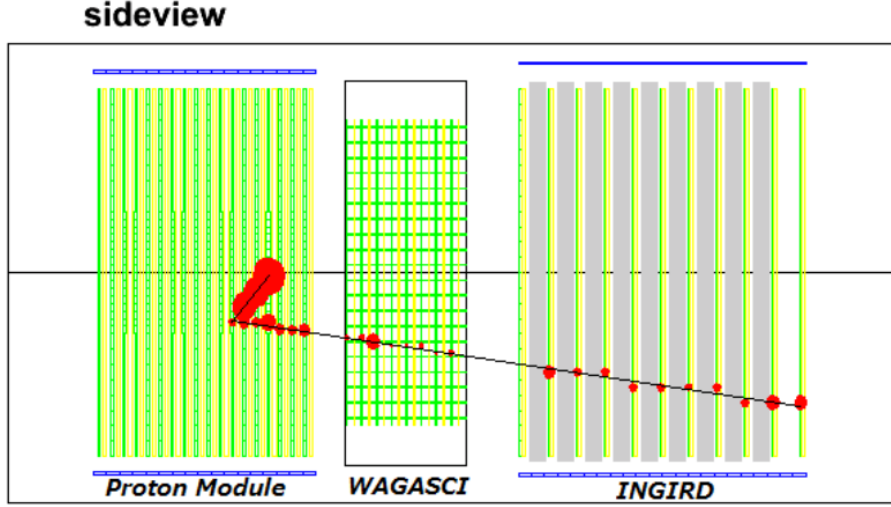


Figure 18: J-PARC T59 event display of a neutrino event in the GENAT4-based detector simulation.

420 **6.1.1 Detector geometry**

421 The detector geometry in the GEANT4-based simulation is slightly different from the
 422 actual detector as shown in Fig. 22. The active neutrino target region consists of four
 423 WAGASCI modules, and each WAGASCI detector has the dimension with $100\text{ cm} \times 100$
 424 cm in the x and y directions and 50 cm along the beam direction. An event display of a
 425 MC event in the WAGASCI detectors is shown in Figure ???. Two Side-MRD modules is
 426 installed at both sides of the WAGASCI modules, and each Side-MRD module consists of
 427 ten iron plates whose dimension is 3 cm (thickness) \times 180 cm (height) \times 320 cm (width).
 428 The distance between the Side-MRD modules and WAGASCI modules is 60 cm. The
 429 downstream-MRD equivalent to the Baby-MIND is installed at the downstream of the
 430 WAGASCI modules. The downstream-MRD consists of ten iron plates whose dimension is
 431 3 cm (thickness) \times 180 cm (height) \times 320 cm (width) and another ten iron plates whose
 432 dimension is 6 cm (thickness) \times 180 cm (height) \times 320 cm (width). The distance between
 433 the downstream-MRD modules and WAGASCI modules is 60 cm.

434 In order to estimate backgrounds from neutrino interactions in the wall and floor of the
 435 experimental hall, the geometry of the experimental hall is implemented in the GEANT4-

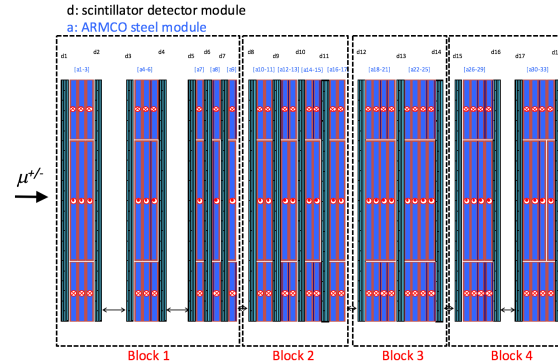
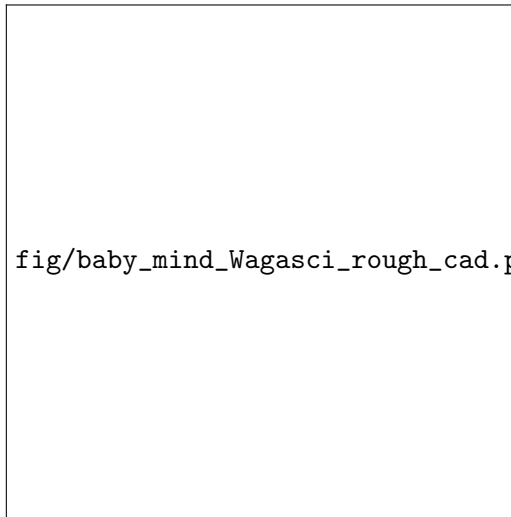


Figure 19: Left) WAGASCI modules: flanked by 2 side muon range detectors (sMRD) and one downstream muon detector (Baby MIND). Right) side view layout of the Baby MIND during beam tests at CERN.

436 based detector simulation.

437 **6.1.2 Response of detector components**

438 The energy deposit inside the scintillator is converted into the number of photons. The
 439 effects of collection and attenuation of the light in the scintillator and the WLS fiber are
 440 simulated, and the MPPC response is also taken into account. The light yield is smeared
 441 according to statistical fluctuations and electrical noise.

442 **6.2 Track reconstruction**

443 To select neutrino interaction from the hit patterns, a track reconstruction algorithm is
 444 developed. The flow of the track reconstruction is as follows.

445 1. Two-dimensional track reconstruction in each sub-detectors

446 2. Track matching among the sub-detectors

447 3. Three -dimensional track reconstruction

448 Add explanation about two-dim reco, track matching and three-dim reco here.

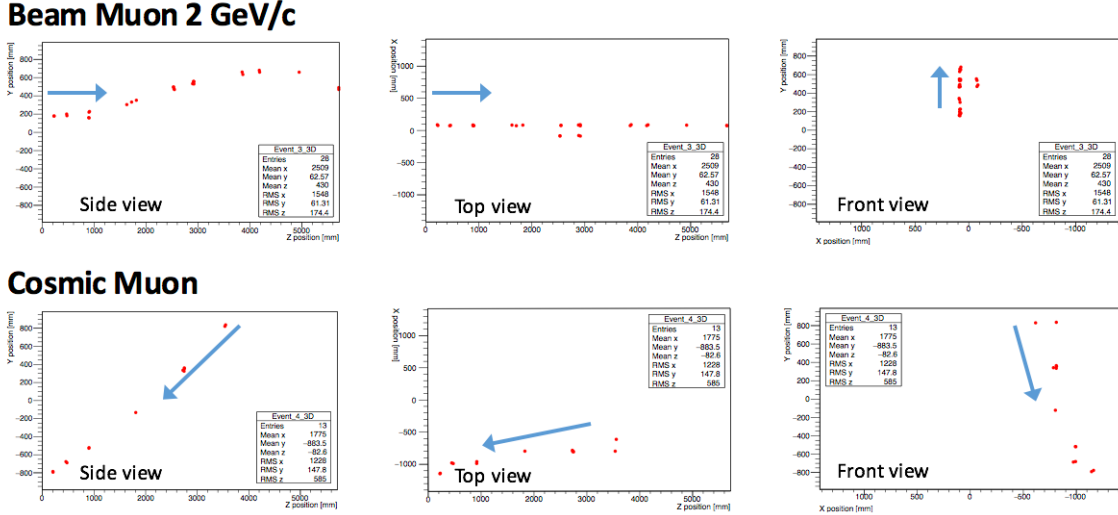


Figure 20: Comparison of a beam muon and cosmic muon in the three different geometrical projections of the detector. The beam impinges on the detector from the left. The arrows indicate the direction of travel of these muons. The direction of the cosmic muon is inferred from timing information.

449 6.3 Event selection

450 First, the events with the track which starts in 5 cm from the wall of the WAGASCI module
 451 are rejected to remove the background from the outside.

452 Second, to reject backgrounds from NC and neutral particles, the longest tracks are
 453 required to penetrate more than one (five) iron plates in Side-MRD modules (Baby-MIND).
 454 Then, in order to measure muon momentum, the longest tracks are required to stop in
 455 MRDs (Side-MRD modules and Baby-MIND) or penetrate all iron plates.

456 Table 1 and 2 show numbers of the selected events after each event election in neutrino-
 457 mode and antineutrino-mode respectively. As for the neutrino-mode, 2.12×10^4 CC events
 458 are expected with 1×10^{21} POT, and the purity is 81.3 %. The main background for
 459 the neutrino-mode is the neutrino interactions in the scintillators inside the WAGASCI
 460 detector. As for the antineutrino-mode, 0.83×10^4 CC events are expected with $1 \times$
 461 10^{21} POT, and the purity is 62.0 %. The main background for the antineutrino-mode
 462 is the wrong sign contamination from ν_μ events and the antineutrino interactions in the
 463 scintillators inside the WAGASCI detector.

464 Figure 23 and 24 show the reconstructed angles of the longest tracks in the selected
 465 events in the neutrino-mode and the anti-neutrino mode respectively.

466 Figure 25 and 26 show the iron plane numbers corresponding to the end points of the
 467 longest tracks in the selected events.

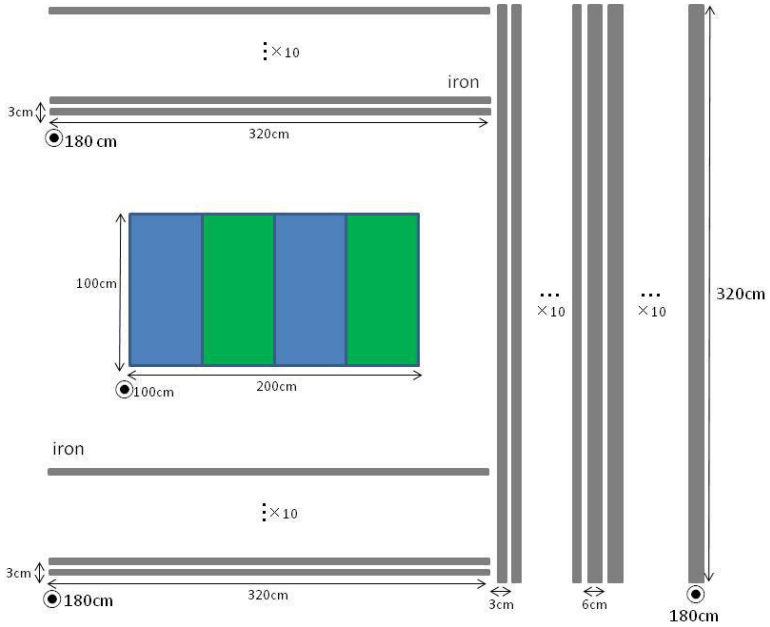


Figure 21: Geometry of the detectors in the Monte Carlo simulation.

468 6.4 Cross section measurements on water

469 In the water target events, the background from interaction with scintillators has to be
470 subtracted by using the measurement of the hydrocarbon target.

471 6.4.1 Charged current cross section measurement

472 7 Standalone WAGASCI-module performances

473 In the previous sections, the WAGASCI detector was studied using the Muon Range De-
474 tectors. In this section, the standalone abilities of WAGASCI module are presented. Using
475 the WAGASCI configuration presented in Section 6, we have evaluated that only 7% of
476 the muons will be stopped in one of the WAGASCI modules. THowerver, this proportion
477 increases to 53% for pions and 73% for protons produced by neutrino interactions at 1.5°
478 off-axis. Figure 27 shows the momentum distribution of these daughter particles as well as
479 for the sub-sample stopped in one of the WAGASCI modules. Therefore, the study of the
480 standalone abilities of the WAGASCI module in this section are dominantly motivated by:

- 481 • the accurate measurement of the neutrino interaction final states. Though most of the

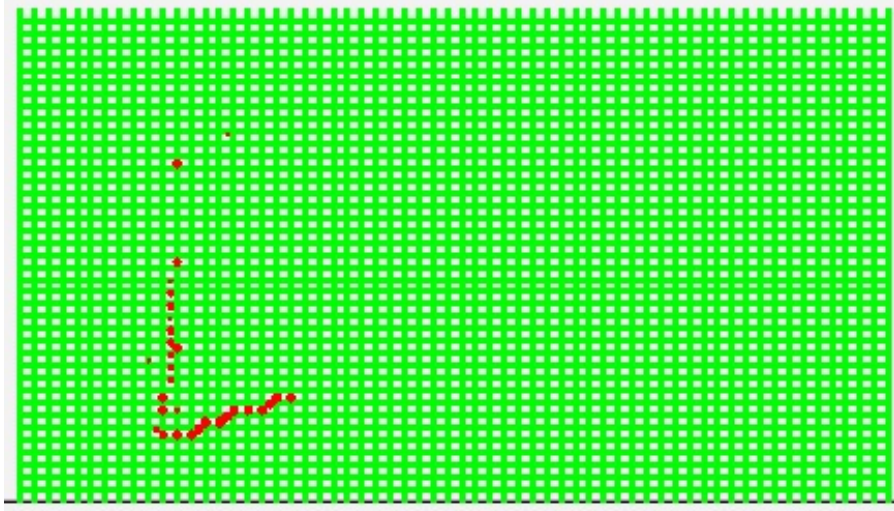


Figure 22: An event display of MC event in WAGASCI detectors. Green lines are scintillators and red circles are the hit channels.

482 muons will be reconstructed and identified in the MRDs, the hadronic particles will
 483 predominantly stops in one WAGASCI module. One has therefore to rely exclusively
 484 on the WAGASCI module information alone to reconstruct, identify and measure the
 485 momentum of pions or protons.

- 486 • the coverage of the MRDs is not 4π . Using the WAGASCI module information can
 487 therefore help to constraint the particles that exits the WAGASCI module but do
 488 not geometrically enters any MRD.
- 489 • the particle identification of low momenta muons $p_\mu < 300 \text{ MeV}/c$ that will leave only
 490 few hits in the MRD. Using the WAGASCI module information will clearly enhance

Table 1: Expected number of the neutrino-candidate events in two WAGASCI modules after the event selections with 1×10^{21} POT in neutrino-mode.

Cut	CC	NC	Scinti Bkg.	Total
Reconstructed	45233	1749.27	9396.46	56378.8
FV	37876.8	1471.02	7869.57	47217.4
Pene. iron	28160.7	593.267	5750.79	34504.7
Stop/Penetrate MRDs	21195.4	534.914	4346.06	26076.4
after all cuts	81.3 %	2.1 %	16.7 %	100 %

Table 2: Expected number of the antineutrino-candidate events in two WAGASCI modules after the event selections with 1×10^{21} POT in antineutrino-mode.

Cut	CC	NC	Scinti Bkg.	Wrong sign bkg	Total
Reconstructed	16249.1	268.082	4468.83	5826.95	26813.0
FV	13644.7	223.211	3746.85	4866.36	22481.0
Pene. iron	10430.8	76.9422	2881.81	3901.35	17290.9
Stop/Penetrate MRDs	8328.73	71.2382	2240.59	2802.98	13443.5
after all cuts	62.0 %	0.5 %	16.7 %	20.9 %	100 %

491 the particle identification.

492 This study is based on an original study done for the ND280 upgrade target, with some
 493 modifications. Though the cell size is similar to the WAGASCI configuration presented
 494 in Section 6, the external dimensions are different ($186.4 \times 60 \times 130$ cm 3). Whenever the
 495 results are presented with this external size and this parameter is likely to impact the
 496 result, it will be mentioned.

497 Note that in this section, a simplified reconstruction algorithm presented in Section 7.1 is
 498 used. The fiducial volume is chosen accordingly as the inner cube of the module which
 499 surfaces are distant of $4 \times$ scintillator space = 10 cm from the module external surfaces.
 500 The neutrino interactions are simulated using NEUT v5.3.2. The NEUT input neutrino
 501 flux is estimated using JnuBeam v13a and assuming the detector to be located at 1.5°
 502 off-axis, as in Section 6. Note that the event reconstruction efficiency as a function of true
 503 neutrino energy might be changed at 1.5° , due for example to different Q^2 distributions. For
 504 this reason, one has to note that the reconstruction results might slightly be changed from
 505 2.5° and 1.5° . To avoid a similar change on the particle-only reconstruction efficiencies,
 506 they will be presented as a function of variables that completely characterize the particle
 507 kinematic state, *i.e.* its momentum and angle. Figure 28 shows the vertices distributions
 508 of the daughter particles of neutrinos interacting one standard WAGASCI water-module.
 509 In this section, we will show the detector reconstruction and particle identification in this
 510 phase space, both for leptonic and hadronic particles. We will finally show an empty
 511 WAGASCI module can highly enhance the ability to constrain the neutrino interaction
 512 final state which is critical to reduce the corresponding uncertainties.

513 7.1 Reconstruction algorithm

514 7.1.1 Description

515 For this section, an ideal “simulated” reconstruction is developed. A particle is recon-
 516 structed if:

- 517 1. The particle is charged.

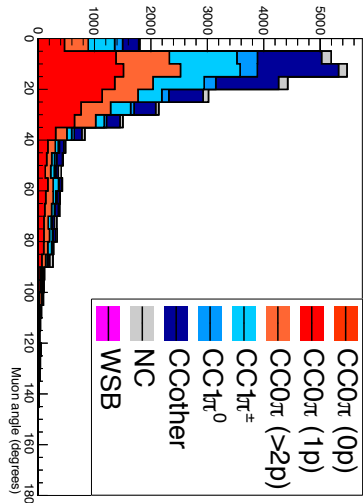


Figure 23: The reconstructed angles of the longest tracks in the selected events in the neutrino-mode.

- 518 2. Lets at least one hit (energy deposit > 2.5 photo-electron) in a scintillator.
 519
 520 3. The particle enters one TPC and let one hit in the tracker.
 521 Or
 522
- 523 • The particle should be long enough to be reconstructed by the detector in at
 524 least 2 out of 3 views (XZ, YZ, XY). The length criterion requires the particle
 525 to let at least 4 hits in the detector. In the “less favourable case” of pure
 526 longitudinal or transverse going tracks, it represents a the track length of $L_{track} \geq$
 527 $4 \times$ scintillator space = 10.0 cm.
 - 528 • In the views where particles pass the length criterion, the particle shall not
 529 be superimposed with longer tracks in at least two views. The superposition
 530 criterion is estimated with the distance inter-tracks (DIT) which corresponds to
 531 the orthogonal distance between two tracks at the ending point of the shortest
 532 one (see Figure 29). For a track 1, the superposition criterion is tested with
 533 every longer tracks that starts at the same vertex. Let \vec{p}_1 the vector of track
 534 1, and p_1^a its projections in the XZ, YZ and XY planes respectively for i=1,2,3.
 535 Note that these are projections in a 2D planes and not on a direction vector. In

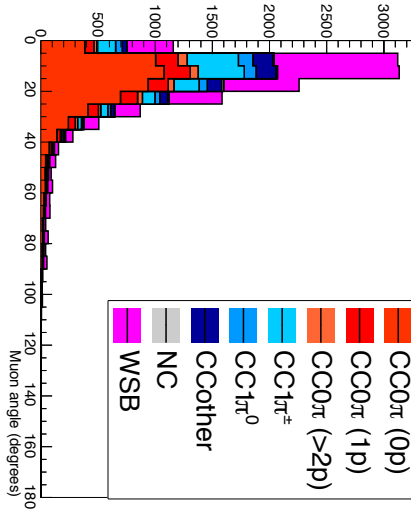


Figure 24: The reconstructed angles of the longest tracks in the selected events in the antineutrino-mode.

536 this case, the relative angle between the track 1 and a longer track 2 (of vector
 537 \vec{p}_2) in a view a is given by:

$$\cos \theta = \frac{\vec{p}_1^a \cdot \vec{p}_2^a}{\|\vec{p}_1^a\| \|\vec{p}_2^a\|} \quad (1)$$

538 and the distance inter track is given by:

$$DIT = \|\vec{p}_1^a\| \sin \theta \quad (2)$$

539 The DIT should be higher than $4 \times$ scintillator width for the track 1 to be not
 540 superimposed with the track 2 in the view a, which also corresponds to 10.0 cm
 541 in the nominal configuration.

542 **7.1.2 Performances**

543 The particle-only reconstruction efficiencies and the reconstruction threshold in momenta
 544 are shown in Table 3. This threshold is defined as the maximal momentum for which the
 545 reconstruction efficiency is smaller than 30%. The thresholds in muon and pion momenta
 546 are 150 MeV/c. Most of the muons are above this threshold (see Figure 28) which leads
 547 to a 79% reconstruction efficiency.

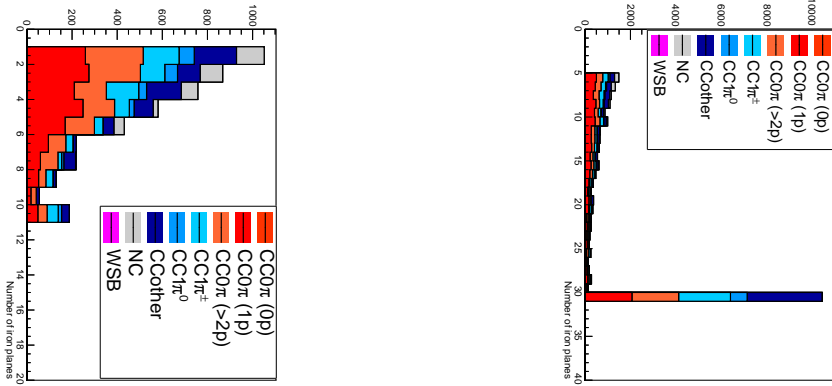


Figure 25: Iron plane numbers in Side-MRD (left) and Baby-MIND (right) corresponding to the end points of the longest tracks in the selected events in the neutrino-mode.

	μ	π	p
Reconstruction Efficiency	79%	52%	26%
Momentum threshold	150 MeV/c	150 MeV/c	550 MeV/c

Table 3: Reconstruction efficiency and momentum threshold for muons, pions and protons. The threshold is defined as the maximal momentum for which particles have a reconstruction efficiency smaller than 30%.

548 The lower pion and proton efficiencies (respectively 52% and 26%) are due to lower
 549 efficiencies for similar momenta than muons, coming from strong interactions as shown
 550 on Figures 30. Efficiencies of each particle type tend to decrease in the backward region
 551 due to particle lower momenta. However, for a fixed momentum value, the reconstruc-
 552 tion efficiency is almost uniform which confirms the ability of the WAGASCI detector to
 553 reconstruct high angle tracks.

554 The reconstruction is thereafter tested on neutrino events. Table 4 summarizes the
 555 number of reconstructed events and efficiencies for each interaction type. As expected
 556 from the high muon reconstruction efficiency, the charged current interactions have recon-
 557 struction efficiencies $\geq 85\%$.

558 The reconstruction efficiencies as a function of the neutrino energy and muon kinematics
 559 are respectively shown on Figure 31 and 32.

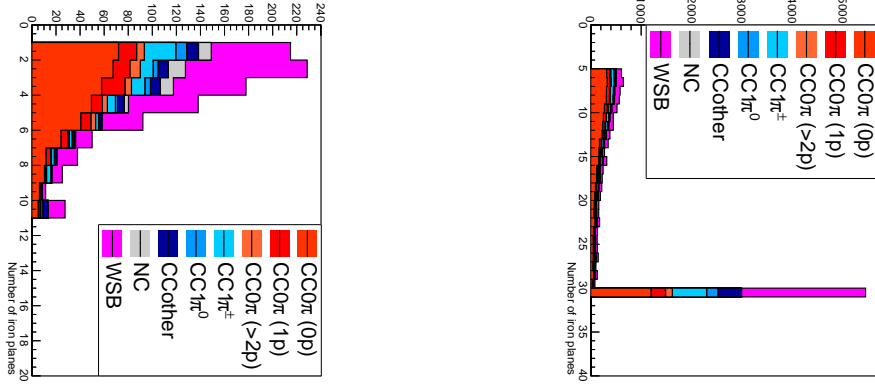


Figure 26: Iron plane numbers in Side-MRD (left) and Baby-MIND (right) corresponding to the end points of the longest tracks in the selected events in the antineutrino-mode.

	CC0 π	CC1 π	CCOthers	NC	All
Reconstruction efficiency	85%	87%	91%	22%	68%

Table 4: Number of true interactions reconstructed. The purity and reconstruction efficiency of each true interaction is also shown.

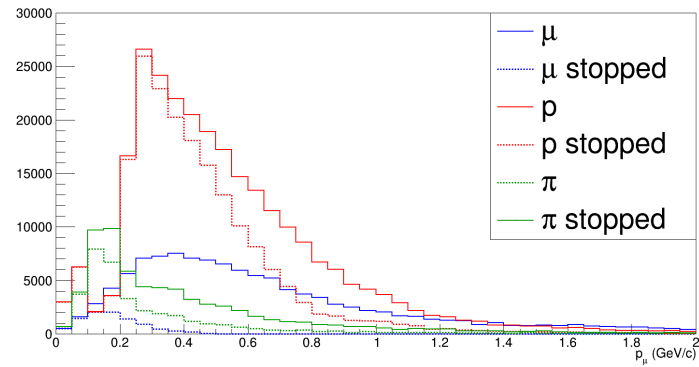


Figure 27: Momentum distribution of true particles in WAGASCI (plain) and corresponding distributions only for particles stopping into the WAGASCI module (dashed).

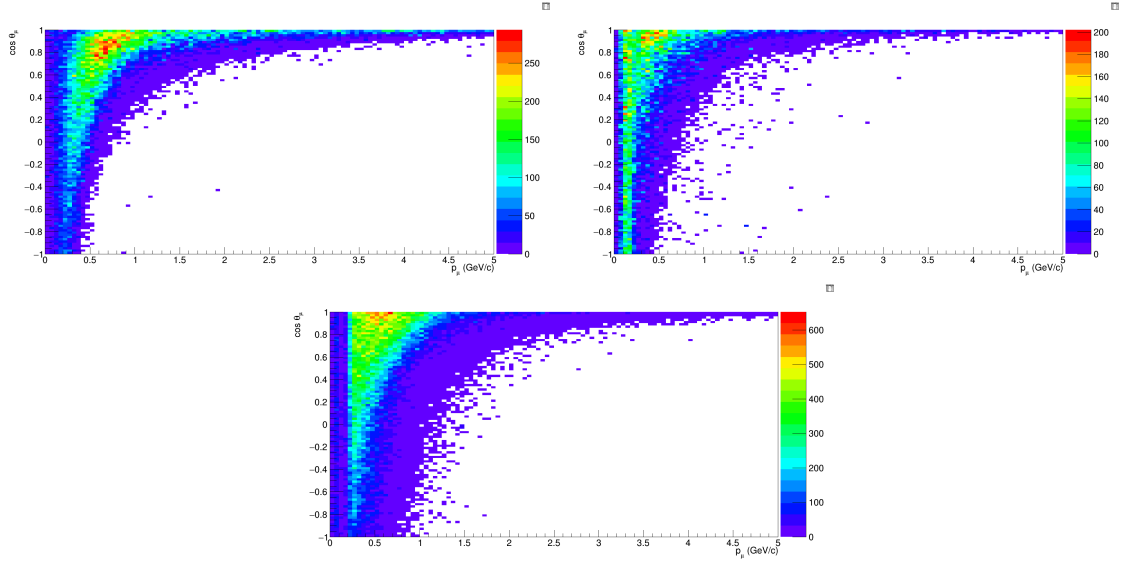


Figure 28: True number of muons (left), charged pions (right) and protons (bottom) in the two WAGASCI water-module as a function of the particles momenta and angles at 1.5° .

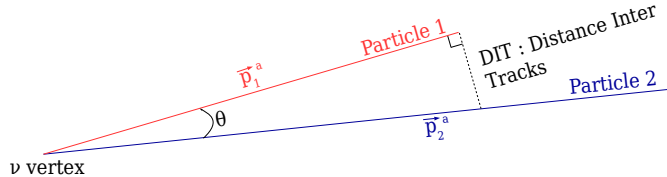


Figure 29: Definition of the distance inter tracks.

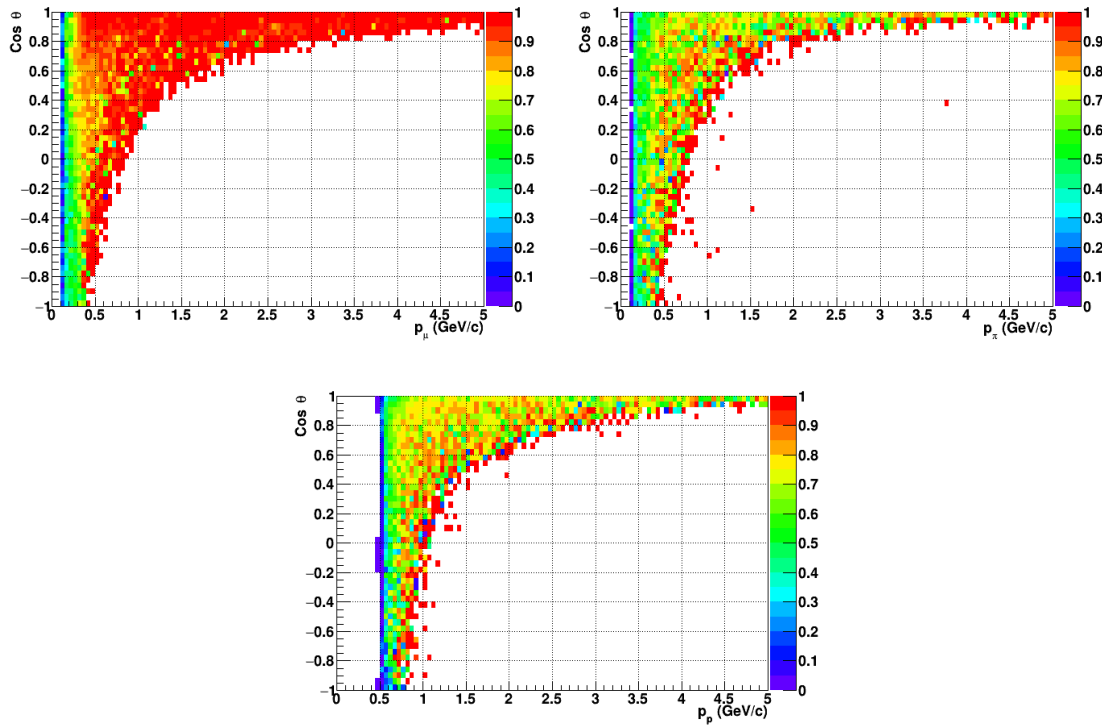


Figure 30: Reconstruction efficiency of muons (left), charged pions (right) and protons (bottom) in the WAGASCI water-module as a function of the particles momenta and angles.

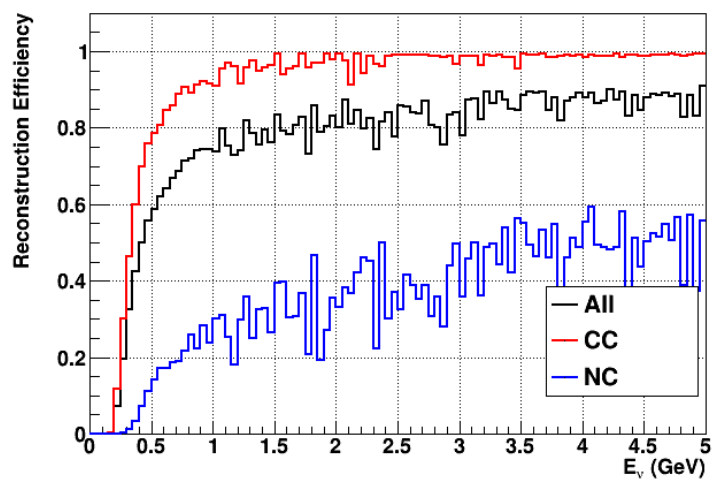


Figure 31: Reconstruction efficiency of all neutrino (black), CC (red) and NC (blue) interactions in the WAGASCI water-module as a function of the neutrino energy.

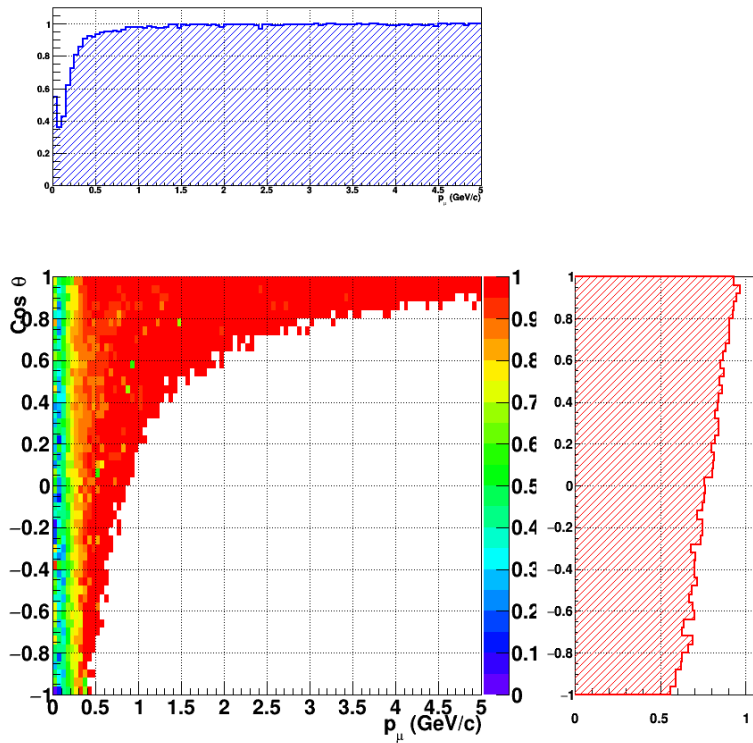


Figure 32: Reconstruction efficiency of CC interactions in the WAGASCI water-module as a function of the muon kinematic variables (momentum and angle).

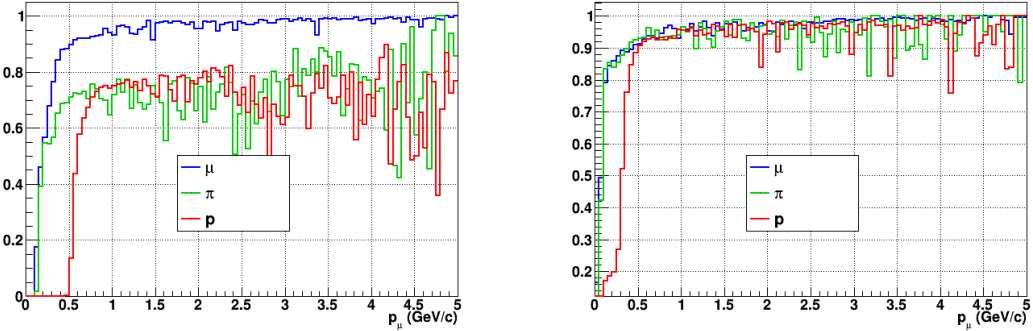


Figure 33: Reconstruction efficiency for muons, pions and protons in the water-in (left) and water-out (right) modules.

560 Note that a Particle Identification Algorithm has been also developed. It is based on
 561 the charge deposition of the particles in the scintillator, of the detection of a decay-electron.
 562 However, this information highly depends on the number of scintillator hit by a particle,
 563 which creates an important difference between a real WAGASCI module and the one used
 564 for the ND280-upgrade simulation. For this reason, the corresponding results will not be
 565 detailed here, but can be found in [?].

566 7.2 Background subtraction: the water-out module

567 In the nominal configuration, 20% of the neutrino interactions occurs on scintillators
 568 (C_8H_8). This background should be removed in order to measure the neutrino interac-
 569 tion on the same target as Super-K, which suppress the differences in cross-section models.
 570 For this purpose, we propose to use a water-out module, where the water is replaced by
 571 air. The detector is therefore fully active and has a 3 mm spatial resolution (scintillator
 572 thickness) which create an ideal detector to reconstruct and identify hadrons, and study
 573 np-nh interactions. The counter-part is the difference in particle energy deposition between
 574 the water and this water-out module that will need to be corrected for. In this section,
 575 we present the capabilities of such a module, and the impact it can have on cross-section
 576 measurements for the neutrino community in general and T2K in particular.
 577 The same reconstruction and selection as the water-in module is applied. Figure 33 shows
 578 the comparison between the water-in and the water-out reconstruction efficiencies for muon,
 579 pions and protons. 90% of the muons and 87% of the pions are reconstructed, while 70%
 580 of the protons are even reconstructed. It allows to lower down the proton threshold to
 581 250 MeV/c (see Table 5).

582 As a consequence of tracking even low momenta particle, the reconstruction efficiency
 583 is uniform and almost maximal on the entire $\cos \theta_\mu$ phase space, as shown on Figure 34.

	μ	π	p
Reconstruction Efficiency Momentum threshold	90% 50 MeV/c	87% 50 MeV/c	70% 250 MeV/c

Table 5: Reconstruction efficiency, proportions of μ -like and non μ -like and momentum threshold for muons, pions and protons in the empty module. The threshold is defined as the maximal momentum for which particles have a reconstruction efficiency smaller than 20%.

584 Since the fiducial mass represents 0.25 tons, the total number of events is divided by a
 585 factor of 3 compared to the water-in module. The water-out module offers interesting
 586 possibilities to study np-nh interaction since 70% of the protons are reconstructed. In the
 587 future, a possible separation as a function of the number of proton track will be studied.
 588 Moreover, we are currently pursuing the use of single and double transverse variables (cite
 589 Xianguo) to open new possibilities for separating np-nh from Final State Interactions, or
 590 for isolating the interactions on hydrogen from interactions on carbon in this module.

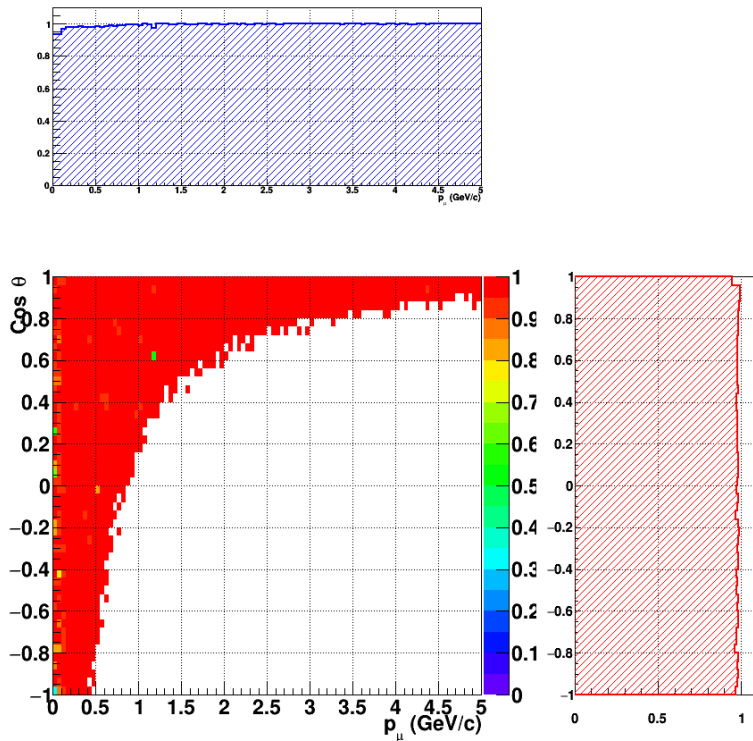


Figure 34: Reconstruction efficiency of CC interactions in the WAGASCI empty module as a function of the muon kinematic variables (momentum and angle).

591 **8 Schedule**

592 We would like to start a physics data taking from T2K beam time after the summer
593 shutdown in 2018. By then, commissioning and tests of the detectors will be completed
594 in J-PARC T59. The experiment can run parasitically with T2K, therefore we request no
595 dedicated beam time nor beam condition as discussed in the following section.

596 Once the approved POT is accumulated, the WAGASCI modules will be removed
597 from the experimental site, but we would like to keep the Baby-MIND and the Side-MRD
598 modules on the B2 floor of the NM pit as common platforms of future neutrino experiments
599 using the T2K neutrino beam.

600 **9 Requests**

601 **9.1 Neutrino beam**

602 The experiment can run parasitically with T2K, therefore we request no dedicated beam
603 time nor beam condition. As data taking periods, we request the ‘nominal’ T2K one-year
604 operation both for the neutrino beam and the antineutrino beam. The T2K has been
605 requesting 0.9×10^{21} POT/year and actually accumulating about 0.7×10^{21} POT/year in
606 recent years. For each year, starting from the Autumn, T2K is running predominantly in
607 the neutrino mode or in the antineutrino mode. Our request is to have one-year neutrino-
608 mode data and another one-year antineutrino mode data assuming that the POT for the
609 fast extraction in each year is more than 0.5×10^{21} POT.

610 **9.2 Equipment request including power line**

611 We request the followings in terms of equipment on the B2 floor:

- 612 • Site for the WAGASCI modules, Side-MRD modules and BabyMIND and their elec-
613 tronics system on the B2 floor of the near detector hall (Fig. 2).
- 614 • Anchor points (holes) on the B2 floor to secure the WAGASCI modules, Side-MRD
615 module and Baby-MIND (Fig. ??)
- 616 • Power line for the magnets in Baby-MIND: 400 V tri-phase 48-to-62 Hz, capable of
617 delivering 12 kW.
- 618 • Electricity for electronics and water circulation system, 3 kW, standard Japanese
619 electrical sockets.
 - 620 1. Online PCs: 2.1 kW
 - 621 2. Electronics: 0.7 kW
 - 622 3. Water sensors: ?

- 623 • Air conditioner for cooling heat generation at Baby-MIND magnets, online PCs and
624 electronics
- 625 • Beam timing signal and spill information
- 626 • Network connection

627 **9.2.1 Baby MIND Equipment request including power line**

628 We request the following in terms of equipment on the B2 floor:

- 629 • Site for the Baby MIND detector and its electronics systems on the B2 floor of the
630 near detector hall.
- 631 • Anchor points (holes) on the B2 floor to secure the 9 support frames, of order 4 holes
632 per frame, detailed floor plans to be communicated in a separate document.
- 633 • Power line for the magnet: 400 V tri-phase 48-to-62 Hz, capable of delivering 12
634 kW. We have a wish for the magnet power line to be installed and available to us by
635 beginning of March 2018.
- 636 • Electricity for electronics, 1 kW, standard Japanese electrical sockets.
- 637 • Beam timing signal and spill information
- 638 • Network connection

639 The infrastructure for much of the above exists already, and will be shared in part with
640 the WAGASCI experiment. Exceptions are the power line for the magnet and holes in the
641 B2 floor to anchor the detector support structures.

642 **10 Conclusion**

643 **References**

- 644 [1] K. Abe et al. Measurement of the muon neutrino inclusive charged-current cross sec-
645 tion in the energy range of 13 GeV with the T2K INGRID detector. *Phys. Rev.*,
646 D93(7):072002, 2016.